Polarization properties of aerosol particles over western Japan: Classification, seasonal variation, and implications for air quality

X.L. Pan[1,2], I. Uno[2], Y. Hara[2], K. Osada[3], S. Yamamoto[4], Z. Wang[2,1], N. Sugimoto[5], H. Kobayashi[6] and Z.F. Wang[1]

[1] Institute of Atmospheric Physics, Chinese Academy of Sciences, Beijing, China

[2] Research Institute for Applied Mechanics, Kyushu University, Kasuga, Japan

[3] Graduate School of Environmental Studies, Nagoya University, Nagoya, Japan

[4] Fukuoka Institute of Health and Environmental Sciences, Daizaifu, Japan

[5] National Institute for Environmental Studies, Ibaraki, Japan

[6] University of Yamanashi, Yamanashi, Japan

Corresponding author: X.L. Pan (panxiaole@mail.iap.ac.cn)

Abstract

Ground-based observation of the polarization properties of aerosol particles using a polarization optical particle counter (POPC) was made from October 27, 2013, to December 31, 2015, at a suburban site in the Kyushu area of Japan. We found that the depolarization ratio (DR, the fraction of s-polarized signal in the total backward light scattering signal) of aerosol particles showed prominent seasonal variability, with peaks in spring (0.21–0.23) and winter (0.19–0.23), and a minimum value (0.09–0.14) in summer. The aerosol compositions in both fine mode (aerodynamic diameter of particle, $D_p < 2.5$ μm) and coarse mode (2.5 μm $< D_p < 10$ μm), and the size-dependent polarization characteristics were analyzed for long-range-transport dust particles, sea salt, and anthropogenic pollution-dominant aerosols. The DR value increased with increasing particle size, and DR = 0.1 was a reliable threshold value to identify the sphericity of supermicron ($D_p > 1$ μm) particles. Occurrence of substandard air quality days in Kyushu was closely related with mixed type (coexistence of anthropogenic pollutants and dust particles in the atmosphere), especially in winter and spring, indicating that dust events in the Asian continent played a key role in the cross-boundary transport of continental pollution. Backward trajectory analysis demonstrated that air masses originating from the western Pacific contained large amounts of spherical particles due to the influence of sea salt, especially in summer; however, for air masses from the Asian continent, the dependence of number fraction of spherical particles on air relative humidity was insignificant, indicating the predominance of less-hygroscopic substances (e.g., mineral dust),

although the mass concentrations of anthropogenic pollutants were elevated.

1. Introduction

The East Asian region is characterized by serious regional anthropogenic pollution, due to the mass consumption of fossil fuel in China (Kurokawa *et al.,* 2013). The region is also influenced by sporadic occurrences of dust plumes from the Taklimakan/Gobi Desert (Uno *et al.,* 2009, Yumimoto *et al.,* 2009). The environmental/climate effects of these anthropogenic and mineral dust aerosols are notably different because of their distinct chemical and physical properties, size distributions, and lifetimes in the troposphere (Pan *et al.,* 2009). Dust aerosols can trap substantial amounts of pollutants (e.g., nitrate), forming a so-called "polluted dust" when they are transported through the planetary boundary layer (PBL) of polluted areas (Wang *et al.,* 2002, Zhang *et al.,* 2005, Zhang *et al.,* 2006). As a consequence, there is substantial variability in their resulting hygroscopic properties, which contributes to considerable uncertainty in predicting their climate effects with models. The light polarization property of a particle is a good proxy indicator of its sphericity/non-sphericity. As such, ground-based light detection and ranging (Lidar) and Cloud-Aerosol Lidar with Orthogonal Polarization (CALIOP) have been developed to derive the attenuated backscattering coefficient at 1064 nm and 532 nm and volume depolarization ratio at 532 nm, the latter of which was used to investigate the temporal and spatial characteristics of dust and pollutant particles in the atmosphere (Shimizu *et al.,* 2004, Winker *et al.,* 2009, Sugimoto and Huang, 2014, Sugimoto *et al.,* 2015). These can be used to investigate the mixed state of dust particles because the data points of pure dust particles are normally in the upper-right portion of a depolarization versus backscattering ratio (1064 nm/532 nm) plot, clearly separate from the data points of pollutant aerosols (in the lower-left portion), with data to the right side of the line connecting the two data clusters reflecting the variation of the mixed state of particles (Sugimoto *et al.,* 2002). Theoretically, the particles with a smaller depolarization ratio (DR, the fraction of *s*-polarized to the total backward scattering, [$S/(S+P)$]) and larger backscattering color ratio may be related to internally mixed Asian dusts; however, this cannot be confidently concluded because the external mixture of dust and large spherical particles (e.g., sea salt) has a similar pattern on the basis of volume backscattering measurements by lidar (Sugimoto *et al.,* 2015).

Recently, a bench-top optical particle counter equipped with a depolarization module was developed. The major advantage of this instrument is its ability to depict the size-resolved polarization of particles (Kobayashi *et al.,* 2014), providing the potential to quantitatively investigate the evolution of the mixing of dust particles during their transport. A study in Seoul (Longitude: 128.95E, Latitude: 37.46N, 116 m a.s.l.) reported the internal mixture of

Asian dust with anthropogenic pollutants on the basis of an evident decrease in the backscattering DR of all particles during a polluted dust episode (Sugimoto *et al.*, 2015). The observation (Pan *et al.,* 2015) of a 7-day dust event in Kyushu in 2014 found that the size-dependent polarization property of particles varied significantly throughout the dust event, and the decrease in the DR of supermicron (aerodynamic diameter of particle, $D_p > 1$ μm) particles was mostly due to an increase in the coarse mode nitrate concentration. This phenomenon was verified by an off-line analysis with transmission electron microscopy (Li and Shao 2009, Li *et al.,* 2011) and a model simulation, which highlighted the direct absorption of nitric acid gas by the dust surface, and/or the volatilization of ammonium nitrate particulate as well as the resulting transfer of nitrate to the dust due to heterogeneous reactions during transport (Allen *et al.,* 2015).

To determine the mixed state of dust particles outflowing from the Asian continent, a long-term field observation was performed at a suburban site in Fukuoka, on the westernmost edge of Japan, beginning in October 2013. The geographic location of the observation site is shown in Figure 1. This location is subject to long-range transport of both anthropogenic pollutions and dust plumes from the Asian continent in spring. Although local emissions (e.g., NO_x) contribute to the nitrate mass, transport is largely responsible for the buildup of $PM_{2.5}$ (particulate matter with a diameter less than or equal to 2.5 μm) in this city (Kaneyasu *et al.,* 2014), particularly during the late winter-spring period. In this study, size-dependent polarization characteristics for single particles were continuously measured by a polarization optical particle counter (POPC), and three common aerosol types (anthropogenic pollutants, dust, and sea salt) were classified, together with an analysis of some key pollutant parameters (sulfate, nitrate, particulate acidity, etc.). The contributions of different aerosol types to ambient aerosol concentrations were investigated. The sphericity/non-sphericity of aerosols from different origins, their relative humidity (RH) dependence, and corresponding impacts on the local air quality in Fukuoka city were investigated using a combined ensemble backward trajectory analysis.

2. Measurements

The light polarization properties of atmospheric aerosol particles (0.5 μm $< D_p < 10$ μm) were measured using a newly developed POPC (YGK Corp., Yamanashi, Japan) at the top of a two-story building at Kyushu University (Longitude: 130.5°E, Latitude: 33.5°N) in Fukuoka prefecture, Japan. We installed a 3 m long vertical stainless steel tube through the roof of the building, and ambient air was drawn into the room with a laminar flow rate of 13 liters per minute (lpm). The loss of coarse mode particles ($D_p > 2.5$ μm) due to gravity settling was negligible. The detailed set-up of the instrumentation is shown in Figure 2. The POPC uses a

780 nm linearly polarized laser source, and measures both forward scattering and backward scattering intensities at 60 degrees and 120 degrees, relative to the direction of incident light. The polarization direction of the incident laser is parallel to the plane of the scattering angle, and the acceptance angle for the polarization detector is 45 degrees (Kobayashi *et al.,* 2014). The sampling rate and half-width of full height (WHFH) of the POPC detector's output signal were 2×10^6 samples/s and ~35 μs, respectively. During the measurements, the pulse signals were sampled during 1 s and processed for 1.2 s. The size of particles is determined from the forward scattering intensity, and two polarized compounds (*s*-polarized/*p*-polarized, polarization direction perpendicular/parallel to the plane of the scattering angle) of backward scattering are measured simultaneously. In practice, the DR is a good indicator of particle sphericity because the direction of polarization of scattered light for spherical particles is identical to that of the incident light, while this is not the case for non-spherical particles (e.g., dust). The DR thresholds for determining the sphericity/non-sphericity of particles are not uniform for different optical instrumentations. For example, lidar observations classify aerosols on the basis of an empirically determined aerosol back-scattering DR (δ_a = S/P), and the values of δ_a <0.02 and δ_a >0.35 (DR = 0.03, 0.26, respectively in this context) are regarded as the thresholds for pure spherical and non-spherical dust particles (Shimizu *et al.,* 2004). Regarding the use of a POPC, Kobayashi et al. (2014) proposed a threshold of DR >0.2 as being "non-spherical" for supermicron particles (e.g., dust) according to the number concentration of particles measured at Fukuoka University. The POPC was calibrated at the observatory every 6 months. The spherical polystyrene standard (Dynospheres, D_p = 0.5 μm, 1 μm, 3 μm, 5 μm, and 10 μm, JSR Life Sciences Corporation) aerosols were generated by a nebulizer at an injection flow rate of 3.5 lpm, and desiccated by passing through a 45 cm Perma casing tube (MD–110–24P, GL Sciences). The overall measurement uncertainty for number density of supermicron particle was less than 15%.

In this study, mass concentrations of particulate matter (PM), sulfate ion (SO_4^{2-}), nitrate ion (NO_3^-), water-soluble organic compounds (WSOC), and particle acidity ($c\Delta H^+$) in both the fine (D_p < 2.5 μm) and coarse mode (2.5 μm < D_p < 10 μm) were simultaneously measured using a continuous dichotomous Aerosol Chemical Speciation Analyzer (ACSA-12, KIMOTO electric Co. Ltd, Osaka, Japan) at 1 h intervals at the observation site. The mass concentration of PM and SO_4^{2-} were determined using the beta-ray absorption method and the $BaSO_4$-based turbidimetric method, respectively, the latter with the addition of $BaCl_2$ dissolved in polyvinylpyrrolidone solution. The mass concentrations of NO_3^- and WSOC were determined with an ultraviolet absorption-photometric method. The $c\Delta H^+$ (nmol/m^3), which refers to the difference of the solution of particles relative to the extracting liquid, was

determined using a pH-indicator absorption-photometric method. The basic equation is $pH_{solution} = -\log [c\Delta H^{+} \times 10^{-6} + 10^{-4.6}]$. Here $pH_{solution}$ is the pH value of aqueous extracts of aerosol sample, and the extract solvent had a pH of 4.6. The details of the ACSA instrument have been published elsewhere (Kimoto *et al.,* 2013).

3. Results

3.1 Temporal variation

The daily (00:00–23:00) averaged volume concentration of particles in different aerosol size bins at the observation site are shown in Figure 3a. In general, the volume concentrations of ambient particles had two pronounced peaks in the fine and/or coarse mode size ranges, particularly in spring and winter. The peak in the fine mode was mostly attributed to anthropogenic pollution, while the coarse mode peak (4–8 μm) was related to mineral dust. The two peaks occurred concurrently or sequentially as a result of different prominent outflow patterns. Itahashi *et al*.(2010) reported that dust and pollution were trapped and well mixed within the PBL, when dust events broke out "behind a cold front," and were characterized by strong stratification. In summer, the volume concentration of particles in both fine and coarse modes decreased significantly because the air masses mostly originated from the western Pacific Ocean where anthropogenic emissions were limited. Wet scavenging processes were significant during summer in Kyushu. The 1 h averaged DR values of particles in each size range during the observation period are shown in Figure 3b. DR value showed a marked increase with increase in particle size, and the dust-impacting episode at the site could be easily identified owing to the distinct increase in the DR value of particles in the fine mode. Due to the clear influence of long-range transport mineral dust at the site, monthly averaged DR values of aerosols in fine mode showed a marked seasonality, with a maximum (~0.14) in spring and minimum (~0.09) in summer (Figure 3c).

3.2 Size distribution

The normalized volume size distribution ($dV/d\log Dp$) of aerosol particles at the site showed prominent seasonal variation (Figure 4). The averaged DR values of each season at the peak size are shown as red circles in the plot. In spring (March, April, and May: MAM), the $dV/d\log Dp$ of particles had a broad peak between 4 μm and 6 μm due to the impact of frequent outbreaks and transport of Asian dust (Figure 4a). The typical DR value at the peak size was 0.21–0.23. In summer (June, July, and August: JJA) the peak size of $dV/d\log Dp$ was 2–3 μm, and the corresponding DR values of particles in the fine mode were less than 0.1. This decrease was mostly due to air masses that originated from clean marine regions and consisted of large amounts of sea salt aerosols, which tend to be spherical under high-

humidity conditions. In autumn, the volume concentrations of particles at the site had their minimum values because of less influence from Asian continent during this season and the meteorological conditions were favorable for proliferation of air pollutants. In winter (December, January, and February: DJF), $dV/d\log Dp$ had two peaks in both the submicron range (D_p = 0.5 μm) and coarse mode (D_p = 4 μm), indicating the combined impact of both anthropogenic pollutants and dust aerosols in the prevailing westerly winds. The DR values at D_p = 0.5 μm and D_p = 4 μm were 0.09 and 0.23, respectively.

It was notable that the observed DR values of particles always showed a marked increase with size in all seasons that was almost independent of aerosol types. This trend was well predicted by an optical model considering particles of Voronoi aggregation (Ishimoto *et al.,* 2010) (SF.1 in Supplementary Information). Theoretical simulation also indicated that an increase in the imaginary part of the refractive index could significantly reduce the DR value; however, from observation, DR values in the coarse mode showed a tendency to increase followed by a leveling off, implying that internal mixture with light-absorbing matter was less important at the site.

Calibration of the POPC using DYNOSHERE (JSR Life Sciences Corp.) aerosols yielded DR values of 0.08, 0.09, and 0.1 for pure spherical particles at D_p = 5 μm, 7 μm, and 10 μm, respectively; and the DR values were almost zero for the particles at D_p = 1 μm, 2 μm, and 3 μm, Nevertheless, in this study, the DR values of aerosols in the coarse modes were 0.2–0.28, much larger than calibration results, indicating that these aerosol particles were generally non-spherical, despite the fact that hygroscopic particles (such as sea salt) may deliquesce and grow under very humid conditions.

4 Discussion

4.1 Size polarization properties for aerosol classification

We classified three distinct aerosol-dominant scenarios based on the mass concentrations of $PM_{2.5}$ and $PM_{2.5\text{-}10}$ (2.5 μm < D_p < 10 μm), and SO_4^{2-} ions in the fine mode (fSO_4^{2-}), and NO_3^- ions in both the fine (fNO_3^-) and coarse modes (cNO_3^-), as shown in Table 1. During anthropogenic pollution-dominant episodes, the mass concentration of $PM_{2.5}$ was 63.4 μg/m^3, which was about five times higher than the $PM_{2.5\text{-}10}$ concentrations (12.9 μg/m^3). The sum of fSO_4^{2-} and fNO_3^- ions accounted for 50% of the total $PM_{2.5}$ mass. During dust-dominant episodes, the mass concentrations of $PM_{2.5}$ and $PM_{2.5\text{-}10}$ were 25.2 and 58.6 μg/m^3, respectively, with minimal contributions from anthropogenic pollutants to the $PM_{2.5}$ mass (fSO_4^{2-} : 1.5 μg/m^3; fNO_3^- : 2.7 μg/m^3). Because we did not measure sodium or chloride ions, a quantitative determination of the influence of sea salt was difficult; however, we could

reasonably assume that during the typhoon period, sea salt aerosol was dominant. Detailed information regarding the trajectory of the two typhoons (No. 1418 Phanfone and No. 1419 Vongfong, SF.2 in Supplementary Information) during the study period is provided on the Japan Meteorological Agency webpage (http://www.data.jma.go.jp/fcd/yoho/typhoon/route_map/index.html). The mass concentrations of $PM_{2.5}$, $PM_{2.5\text{-}10}$, fSO_4^{2-}, and fNO_3^- were small during the typhoon period with mean values of 5.3 μg/m^3, 4.9 μg/m^3, 0.4 μg/m^3, and 1.5 μg/m^3, respectively.

To identify the polarization characteristics for the different aerosol types, the volume concentration of particles at different depolarization ratios and particle sizes during specific periods were plotted (Figure 5). To aid comparison, the volume concentration in the plot was normalized to a maximum value = 1 using the equation: (*value* – *min*)/(*max* – *min*) (hereafter; referred to as a DR-D_p-Volume plot). We divided the plot into four subregions. The plot shows that anthropogenic pollution-dominant aerosols were mostly in the submicron range, with DR values < 0.2 (marked as region "A1," in Figure 5a). Mineral-dust-dominant aerosols had a larger diameter (D_p > 4 μm) and a non-spherical morphology associated with a DR value of 0.4 (marked as region "A2," in Figure 5b). Sea-salt-dominant aerosols were in the supermicron range, with DR values < 0.1 (marked as region "A3," in Figure 5c). During the typhoon period, we considered the sea salt particles to be spherical because sea salt occurs as entirely liquid drops when RH >75% (Wise *et al.,* 2007). Based on this information, we proposed a DR threshold value of 0.1 to distinguish between spherical and non-spherical particles in the supermicron size range. This criterion was consistent with the theoretical Mie-scattering calculation and classification in the literature (Kobayashi *et al.,* 2014). The sphericity/non-sphericity of submicron particles with DR > 0.2 was not considered because of the low volume concentration. With regard to A1, we cannot be specific about the sphericity/non-sphericity of the particles because the morphology of anthropogenic particles is extremely variable, and depends on the mass fractions of carbonaceous matter and water-soluble inorganics, as well as meteorological conditions (e.g., RH), the mixed state, and the degree of atmospheric aging (Li *et al.,* 2011, Fu *et al.,* 2012). Additionally, the *s*-polarized backscattering of submicron particles decreased significantly with a decrease in their size on the basis of theoretical simulations, even for non-spherical particles (Sugimoto *et al.,* 2015).

4.2 Contributions of different aerosol types to local air quality

Using the criteria suggested in Section 4.1, we investigated the impacts of different aerosol types on local air quality in western Japan. The period when the DR-D_p -volume plot had only one prominent volume mode in A1 with mode DR value > 0.1 was considered anthropogenic-pollution-dominant. The dust-dominant period was characterized by a distinct

volume mode in "A2" and mode DR value > 0.3. Periods when three distinct modes occurred simultaneously in A1, A2, and A3 were considered to represent a "mixed type"(Figure 5d). Determination of the sea-salt-dominant period was based on two distinct volume modes in the fine mode, and small DR values (<0.1). A scenario in which the DR-D_p-volume plot had only two volume modes in both A2 and A3 was also observed during a long-lasting dust event at the end of May 2015 (Pan *et al.,* 2015); we considered this as "dust dominant."

Monthly-averaged and median mass concentrations of $PM_{2.5}$ and $PM_{2.5-10}$ in 2014 and 2015 are shown in Figure 6a. In general, ambient $PM_{2.5}$ levels displayed a clear winter-spring high and summer low. In contrast, the mass concentrations of $PM_{2.5-10}$ had a pronounced peak in May, reflecting frequent dust events. The average monthly values were generally larger than the median values during spring, indicating that the observation site was influenced by several intensive pollution events. Figure 6b depicts the number of substandard days that the daily-averaged mass concentration of $PM_{2.5}$ exceeded the National Ambient Air Quality Standard (NAAQS) of Japan (35 $\mu g/m^3$) in each month during the observation period. It can be seen that the greatest number of substandard days (12) occurred in May 2014, and mixed type pollutants were responsible for about 60% of these substandard days, followed by dust-dominant types (25%). It is notable that the number of substandard days in a month was closely correlated with the number fraction of "mixed type" pollution during winter and spring. This indicates that air quality in western Japan was influenced mainly by long-range transport of dust and pollution mixed aerosols from the Asian continent. Cross-boundary transport of anthropogenic pollutants during dust events has been reported in several previous studies (Takemura *et al.,* 2002, Shin *et al.,* 2015). The influence of dust-dominant aerosol was generally less than 5% over the course of 1 year. Anthropogenic pollution-dominant cases were mostly responsible for substandard days in summer, although only a few such days were observed during the study period.

It was notable that the monthly-averaged mass concentrations of $PM_{2.5}$ in winter (23.7 ± 4.3 $\mu g/m^3$) and spring (27 ± 3.8 $\mu g/m^3$) of 2014 were greater than those (20.9 ± 1.9 $\mu g/m^3$ and 20.4 ± 1.5 $\mu g/m^3$) in 2015, and that the number of substandard days in 2014 was also higher than that in 2015. This implies that transport from the Asian continent was relatively intensive in 2014. The causes of this difference in variation in regional synoptic weather conditions and emissions inventories provide important topics for future studies.

4.3 Polarization properties of aerosols from different origins

The DR-D_p-volume plots of aerosol particles from different geographical origins were evaluated in combination with a backward trajectory analysis (Figure 7). The footprint

regions for air masses were determined based on ensemble simulations of 5-day backward trajectories of air parcels using the Hybrid Single Particle Lagrangian Integrated Trajectory (HYSPLIT) model (v4.9; available at http://ready.arl.noaa.gov/HYSPLIT.php), offsetting the release point by a meteorological grid point in the horizontal and 0.01 sigma units in the vertical. Therefore 27 trajectories were calculated simultaneously in each hour. We divided the region of interest into four sub-regions, where the emission intensity of pollutants and aerosol types were different. In Region I (Figure 7a), which mostly covered the Japanese landmass, the DR-D_p -volume plot had one predominant peak at MDR = 0.05 and D_p = 1.8 μm (Figure 7b). The small polarization degree of aerosol particles in the fine mode indicated that the aerosol particles tended to be spherical. Only 2% of this period was found to have substandard air quality. When the air mass came from Region II which included the polluted region of northern China and the Korean Peninsula (Figure 7c) the volume concentrations of particles in all size bins increased significantly, and the volume size distributions of particles had three distinct modes at D_p = 0.7 μm (MDR = 0.1), D_p = 1.9 μm (MDR = 0.08), and D_p = 5 μm (MDR = 0.35) (Figure 7d). The volume peaks in the coarse modes could be attributed to long-range transport of mineral dust. We found that 32% of the days, dominated by northwesterly winds, were substandard, i.e., anthropogenic-pollutant-dominant, mineral-dust-dominant, and mixed-type-dominant aerosols contributed to 13%, 8%, and 11% of period, respectively. When air masses came from Region III (East China Sea, Figure 7e), 92% of these days met the NAAQS for Japan, and substandard days were mostly related to anthropogenic pollution (9%). The MDR (0.03) for supermicron particles was very small (Figure 7f), indicating a high degree of sphericity. Air masses from Region VI (western Pacific Ocean, Figure 7g) also contained a large volume fraction of supermicron particles, with small MDR values (~0.03). We found that substandard air quality days (16% of all days), when air masses came from Region VI, were more frequent than for Region III, reflecting the mixing of maritime air with local anthropogenic emissions over the western part of Japan (Figure 7g). It should be noted that the air masses arriving from different regions displayed distinct seasonality (Table 2), and that the acidities of particles in the coarse mode ($c\Delta H^+$) showed a marked difference. Air masses from Region I were concentrated in summer and autumn ($c\Delta H^+$ = 3.6 ± 1.4 nmol/m^3). Air masses from Region II occurred more frequently in winter ($c\Delta H^+$ = -4.7 ± 1.0 nmol/m^3) and spring ($c\Delta H^+$ = -2.8 ± 1.0 nmol/m^3), and the negative $c\Delta H^+$ indicated that the air masses contained of alkaline substances (Ca^{2+}, Mg^{2+} etc.) Air masses from Region III ($c\Delta H^+$ = 2.0 ± 3.0 nmol/m^3) and Region IV ($c\Delta H^+$ = 7.5 ± 4.9 nmol/m^3) occurred only in summer. Overall, the DR-D_p-volume plots in Figure 8 provide an accurate representation of the polarization characteristics of particles from different regions.

4.4 Fraction of spherical particles as a function of RH

As mentioned in previous studies (Koehler *et al.,* 2009, Sullivan *et al.,* 2009), the more dust particles become involved in chemical mixing, the more easily they become hydrophilic and are incorporated into cloud processes, which results in complicated climate effects. Here, the hygroscopicity of aerosol particles from different regions was investigated on the basis of the number fraction of particles with DR <0.1 (referred to as "$NFP_{DR<0.1}$") as a function of the averaged RH, which was calculated along 3-day backward trajectories (Figure 8). The dataset period when intensive precipitation (>20 mm/hr) occurred along the trajectories was removed. The averaged RH of air masses from Regions III and IV were relatively high (>70%) because of their longer stagnancy in the marine area. For particles with $1.0 < D_p < 1.5$ μm (Figure 8a), the $NFP_{DR<0.1}$ was positively correlated with the RH for particles from all origins. This phenomenon can be explained by the coexistence of hygroscopic masses such as sulfate and nitrate. About 70% of particles were probably spherical in the air mass from Region I, and this figure increased to 89% at RH = 76%. In the air masses from Region II, $NFP_{DR<0.1}$ was 62% at RH = 45% and increased slightly to 72% at RH = 82%. For coarse-mode particles (Figure 8b) from Region II, the $NFP_{DR<0.1}$ was ~32%, irrespective of RH. The chemical analysis indicated that the mass fraction of water-soluble matter in coarse-mode particles (WSM = cSO_4^{2-} + cNO_3^- + cWSOC) from Region II was 15%, similar to that of air masses from other origins. The missing part in mass balance was likely to be related to crustal species (Pan *et al.,* 2009). When the air mass came from Region II, in about 78% of trajectories the acidities of particles were negative with a mean of -4.4 ± 3.1 nmol/m^3, indicating that the particles contained of crustal substances. $c\Delta H^+$ values of particles from other regions were normally positive (as shown in Table 2). This difference also partially explains the weaker hygroscopicity of particles from Region II compared to other regions. The $NFP_{DR<0.1}$ from Regions I and III were still very sensitive to the variation in RH, which suggested that the large aerosol particles were related to hygroscopic aerosols.

5 Conclusions

We conducted continuous observations of the polarization properties and chemical composition of aerosol particles in Kyushu during 2014–2015, using a POPC and ACSA-12. The conclusions are as follows: (1) POPC could objectively identify anthropogenic-pollutant-dominant, mineral-dust-dominant, and sea-salt-dominant aerosol types from their distinct depolarization ratio-size characteristics. We suggest that a DR of 0.1 is a reliable threshold that can be used to classify the sphericity/non-sphericity of supermicron particles. (2) We

found that LRT dust and pollution mixed events were mainly responsible for substandard air quality days in western Japan in spring and winter. In summer, particles in the coarse mode at the observation site were mostly spherical due to the impact of sea salt at high RH conditions. (3) The correlation between the number fraction of spherical particles with DR <0.1 ($NFP_{DR<0.1}$) and RH for coarse-mode particles from Region II was not significant because of the existence of non-hydrophilic materials (i.e., dust). Nevertheless, there was a clear positive correlation between $NFP_{DR<0.1}$ and RH for particles from Regions III and IV, implying a significant impact of sea salt. (4) Local emissions were partially responsible for the occurrence of substandard air quality days in Kyushu, occurring mainly in summer.

Acknowledgments

This work was supported by a Grant-in-Aid for Scientific Research (25220101) from the Japan Society for the Promotion of Science (JSPS). To request POPC data for scientific research purposes, please contact Prof. Itsushi Uno at Kyushu University via email (uno@riam.kyushu-u.ac.jp).

References

Allen H. M., Draper D. C., Ayres B. R., Ault A., Bondy A., Takahama S., Modini R. L., Baumann K., Edgerton E., Knote C. Influence of crustal dust and sea spray supermicron particle concentrations and acidity on inorganic NO 3− aerosol during the 2013 Southern Oxidant and Aerosol Study. Atmospheric Chemistry and Physics. 15(18):10669-85, 2015.

Dubovik O., Sinyuk A., Lapyonok T., Holben B. N., Mishchenko M., Yang P., Eck T. F., Volten H., Munoz O., Veihelmann B. Application of spheroid models to account for aerosol particle nonsphericity in remote sensing of desert dust. Journal of Geophysical Research: Atmospheres (1984–2012). 111(D11), 2006.

Fu H., Zhang M., Li W., Chen J., Wang L., Quan X., Wang W. Morphology, composition and mixing state of individual carbonaceous aerosol in urban Shanghai. Atmospheric Chemistry and Physics. 12(2):693-707, 2012.

Itahashi S., Yumimoto K., Uno I., Eguchi K., Takemura T., Hara Y., Shimizu A., Sugimoto N., Liu Z. Structure of dust and air pollutant outflow over East Asia in the spring. Geophysical Research Letters. 37(20), 2010.

Ishimoto H., Zaizen Y., Uchiyama A., Masuda K., Mano Y. Shape modeling of mineral dust particles for light-scattering calculations using the spatial Poisson–Voronoi tessellation. Journal of Quantitative Spectroscopy and Radiative Transfer. 111(16):2434-43, 2010.

Kaneyasu N., Yamamoto S., Sato K., Takami A., Hayashi M., Hara K., Kawamoto K., Okuda T., Hatakeyama S. Impact of long-range transport of aerosols on the PM2.5 composition at a major metropolitan area in the northern Kyushu area of Japan. Atmospheric Environment.416-25, 2014.

Kimoto H., Ueda A., Tsujimoto K., Mitani Y., Toyazaki Y., Kimoto T. Development of a Continuous Dichotomous Aerosol Chemical Speciation Analyzer. Clean Technology. 23:49-52, 2013.

Kobayashi H., Hayashi M., Shiraishi K., Nakura Y., Enomoto T., Miura K., Takahashi H., Igarashi Y., Naoe H., Kaneyasu N. Development of a polarization optical particle counter capable of aerosol type classification. Atmospheric Environment.486-92, 2014.

Koehler K. A., Kreidenweis S. M., DeMott P. J., Petters M. D., Prenni A. J., Carrico C. M. Hygroscopicity and cloud droplet activation of mineral dust aerosol. Geophysical Research Letters. 36(8), 2009.

Kurokawa J., Ohara T., Morikawa T., Hanayama S., Janssens-Maenhout G., Fukui T., Kawashima K., Akimoto H. Emissions of air pollutants and greenhouse gases over Asian regions during 2000–2008: Regional Emission inventory in ASia (REAS) version 2. Atmospheric Chemistry and Physics. 13(21):11019-58, 2013.

Li W. J., Shao L. Y. Observation of nitrate coatings on atmospheric mineral dust particles. Atmospheric Chemistry and Physics. 9(6):1863-71, 2009.

Li W. J., Zhang D. Z., Shao L. Y., Zhou S. Z., Wang W. X. Individual particle analysis of aerosols collected under haze and non-haze conditions at a high-elevation mountain site in the North China plain. Atmospheric Chemistry and Physics. 11(22):11733-44, 2011.

Ohara T., Akimoto H., Kurokawa J., Horii N., Yamaji K., Yan X., Hayasaka T. An Asian emission inventory of anthropogenic emission sources for the period 1980-2020. Atmos Chem Phys. 7(16):4419-44, 2007. 10.5194/acp-7-4419-2007

Pan X. L., Uno I., Hara Y., Kuribayashi M., Kobayashi H., Sugimoto N., Yamamoto S., Shimohara T., Wang Z. Observation of the simultaneous transport of Asian mineral dust aerosols with anthropogenic pollutants using a polarization optical particle counter (POPC) during a long-lasting dust event in late spring 2014. Geophysical Research Letters.2014GL062491, 2015. 10.1002/2014GL062491, 2015

Pan X. L., Yan P., Tang J., Ma J. Z., Wang Z. F., Gbaguidi A., Sun Y. L. Observational study of influence of aerosol hygroscopic growth on scattering coefficient over rural area near Beijing mega-city. Atmospheric Chemistry and Physics. 9(19):7519-30, 2009.

Shimizu A., Sugimoto N., Matsui I., Arao K., Uno I., Murayama T., Kagawa N., Aoki K., Uchiyama A., Yamazaki A. Continuous observations of Asian dust and other aerosols by polarization lidars in China and Japan during ACE□Asia. Journal of Geophysical Research: Atmospheres (1984–2012). 109(D19), 2004.

Sugimoto N., Huang Z. Lidar methods for observing mineral dust. Journal of Meteorological Research. 28(2):173-84, 2014.

Sugimoto N., Matsui I., Shimizu A., Uno I., Asai K., Endoh T., Nakajima T. Observation of dust and anthropogenic aerosol plumes in the northwest Pacific with a two-wavelength polarization lidar on board the research vessel Mirai. Geophysical Research Letters. 29(19):7-1-7-4, 2002.

Sugimoto N., Nishizawa T., Shimizu A., Matsui I., Kobayashi H. Detection of internally mixed Asian dust with air pollution Aerosols using a polarization optical particle counter and a polarization-sensitive two-wavelength

lidar. Journal of Quantitative Spectroscopy and Radiative Transfer. 150:107-13, 2015. 10.1016/j.jqsrt.2014.08.003

Shin S. K., Müller D., Lee C., Lee K. H., Shin D., Kim Y. J., Noh Y. M. Vertical variation of optical properties of mixed Asian dust/pollution plumes according to pathway of air mass transport over East Asia. Atmos Chem Phys. 2015.

Sullivan R. C., Moore M. J. K., Petters M. D., Kreidenweis S. M., Roberts G. C., Prather K. A. Effect of chemical mixing state on the hygroscopicity and cloud nucleation properties of calcium mineral dust particles. Atmospheric Chemistry and Physics. 9(10):3303-16, 2009.

Tobo Y., Zhang D., Matsuki A., Iwasaka Y. Asian dust particles converted into aqueous droplets under remote marine atmospheric conditions. Proceedings of the National Academy of Sciences. 107(42):17905-10, 2010.

Takemura T., Uno I., Nakajima T., Higurashi A., Sano I. Modeling study of long‐range transport of Asian dust and anthropogenic aerosols from East Asia. Geophysical Research Letters. 29(24), 2002.

Uno I., Eguchi K., Yumimoto K., Takemura T., Shimizu A., Uematsu M., Liu Z., Wang Z., Hara Y., Sugimoto N. Asian dust transported one full circuit around the globe. Nature Geoscience. 2(8):557-60, 2009.

Wang Z., Akimoto H., Uno I. Neutralization of soil aerosol and its impact on the distribution of acid rain over east Asia: Observations and model results. Journal of Geophysical Research: Atmospheres (1984–2012). 107(D19):ACH 6-1-ACH 6-12, 2002.

Winker D. M., Vaughan M. A., Omar A., Hu Y., Powell K. A., Liu Z., Hunt W. H., Young S. A. Overview of the CALIPSO mission and CALIOP data processing algorithms. Journal of Atmospheric and Oceanic Technology. 26(11):2310-23, 2009.

Wise M. E., Semeniuk T. A., Bruintjes R., Martin S. T., Russell L. M., Buseck P. R. Hygroscopic behavior of NaCl-bearing natural aerosol particles using environmental transmission electron microscopy. Journal of Geophysical Research: Atmospheres (1984–2012). 112(D10), 2007.

Yumimoto K., Eguchi K., Uno I., Takemura T., Liu Z., Shimizu A., Sugimoto N. An elevated large-scale dust veil from the Taklimakan Desert: Intercontinental transport and three-dimensional structure as captured by CALIPSO and regional and global models. Atmospheric Chemistry and Physics. 9(21):8545-58, 2009.

Zhang D., Iwasaka Y., Matsuki A., Ueno K., Matsuzaki T. Coarse and accumulation mode particles associated with Asian dust in southwestern Japan. Atmospheric Environment. 40(7):1205-15, 2006.

Zhang D., Iwasaka Y., Shi G., Zang J., Hu M., Li C. Separated status of the natural dust plume and polluted air masses in an Asian dust storm event at coastal areas of China. Journal of Geophysical Research: Atmospheres (1984–2012). 110(D6), 2005.

444 **List of Tables**

445 Table 1. Statistics for the mass concentrations of $PM_{2.5}$, $PM_{2.5-10}$, fSO_4^{2-}, fNO_3^-, and cNO_3^- for
446 three distinct aerosol-dominant periods.

Classification	Date Time	$PM_{2.5}$ (μg/m³)	$PM_{2.5-10}$ (μg/m³)	fSO_4^{2-} (μg/m³)	fNO_3^- (μg/m³)	cNO_3^- (μg/m³)
Anthropogenic-pollution-dominant period (n = 12)	2014-01-12 19:00	71.7	16.9	11.5	18.0	3.5
	2014-01-13 01:00	63.6	13.1	10.5	18.9	2.6
	2014-01-13 03:00	61.0	11.8	10.4	17.7	2.9
	2014-01-13 07:00	56.3	11.9	10.0	17.7	2.7
	2014-01-13 10:00	60.4	13.1	10.5	16.2	2.6
	2014-01-17 20:00	61.5	16.2	12.1	17.0	3.1
	2014-01-17 21:00	62.3	13.5	12.0	16.4	3.1
	2014-01-18 03:00	52.4	11.4	11.1	17.0	2.4
	2014-01-18 06:00	56.4	10.8	11.8	19.3	2.5
	2014-01-18 11:00	68.7	13.2	12.7	15.3	3.0
	2014-01-20 18:00	74.5	11.0	15.2	16.8	3.1
	2014-01-26 03:00	72.3	11.9	10.6	16.2	2.6
	Average	63.4	12.9	11.5	17.2	2.8
	S. D.	7.0	1.9	1.4	1.2	0.3
Mineral-dust-dominant period (n=8)	2014-01-01 17:00	22.4	55.4	2.2	2.8	3.8
	2014-01-01 18:00	23.8	52.2	1.9	2.4	2.7
	2014-01-01 21:00	25.6	51.4	1.8	2.9	2.4
	2014-05-18 10:00	25.7	54.5	1.2	2.8	1.6
	2014-05-18 11:00	23.9	63.1	0.9	2.5	1.4
	2014-05-18 12:00	30.0	74.7	1.2	2.7	1.4
	2014-05-18 13:00	35.8	81.3	1.2	3.0	1.6
	Average	25.2	58.6	1.5	2.7	2.2
	S. D.	2.6	8.9	0.5	0.2	0.9
Typhoon period (n=13)	2014-10-05 03:00	6.8	9.4	0.5	1.6	0.5
	2014-10-05 05:00	7.4	8.4	0.5	1.1	0.4
	2014-10-05 06:00	7.2	9.8	0.6	1.3	0.4
	2014-10-05 08:00	7.6	9.0	0.6	1.7	0.4
	2014-10-05 09:00	6.6	8.6	0.6	2.0	0.5
	2014-10-13 02:00	6.2	3.3	0.5	2.5	0.3
	2014-10-13 03:00	5.0	1.8	0.5	2.4	0.3
	2014-10-13 04:00	5.7	3.6	0.3	1.8	0.4
	2014-10-13 05:00	4.5	2.6	0.4	0.9	0.6
	2014-10-13 06:00	2.9	1.5	0.3	1.0	0.8
	2014-10-13 07:00	1.8	0.3	0.3	0.3	0.4
	2014-10-13 08:00	1.5	1.0	0.3	0.9	0.3
	2014-10-13 09:00	2.6	0.1	0.2	0.5	0.2
	Average	5.3	4.9	0.4	1.5	0.4
	S. D.	2.2	3.7	0.1	0.7	0.1

447

448 Table 2. Number counts of trajectories used in Figure 7 and corresponding monthly averaged
449 acidities of particles ($c\Delta H^+$) in coarse mode for different regions. Hyphens indicate the
450 months when the number counts of trajectories are <10.
451

Month (2014)	Region I		Region II		Region III		Region IV	
	Num.	$c\Delta H^+$ (nmol/m^3)	Num.	$c\Delta H^+$ (nmol/m^3)	Num.	$c\Delta H^+$ (nmol/m^3)	Num.	$c\Delta H^+$ (nmol/m^3)
Jan	-	-	203	-5.2 ± 4.5	-	-	-	-
Feb	-	-	108	-5. 3 ± 2.4	-	-	-	-
Mar	-	-	114	-1.8 ± 2.6	-	-	-	-
Apr	-	-	175	-3.0 ± 3.4	18	-1.4 ± 2.4	-	-
May	-	-	276	-3.5 ± 6.7	-	-	-	-
Jun	102	3.7 ± 2.5	69	3.4 ± 2.5	-	-	14	13.2 ± 16.7
Jul	34	2.5 ± 1.3	33	4.7 ± 3.1	-	-	85	4.2 ± 3.8
Aug	132	4.8 ± 2.9	-	-	136	1.5 ± 3.1	71	5.1 ± 2.7
Sep	22	2.4 ± 3.6	-	-	104	5.9 ± 2.7	-	-
Oct	26	4.7 ± 3.7	107	1.1 ± 4.3	-	-	-	-
Nov	-	-	629	-1.7 ± 4.4	-	-	-	-
Dec	12	-5.9 ± 1.3	527	-3.7 ± 1.8	-	-	-	-

452

453 **List of Figures**

454

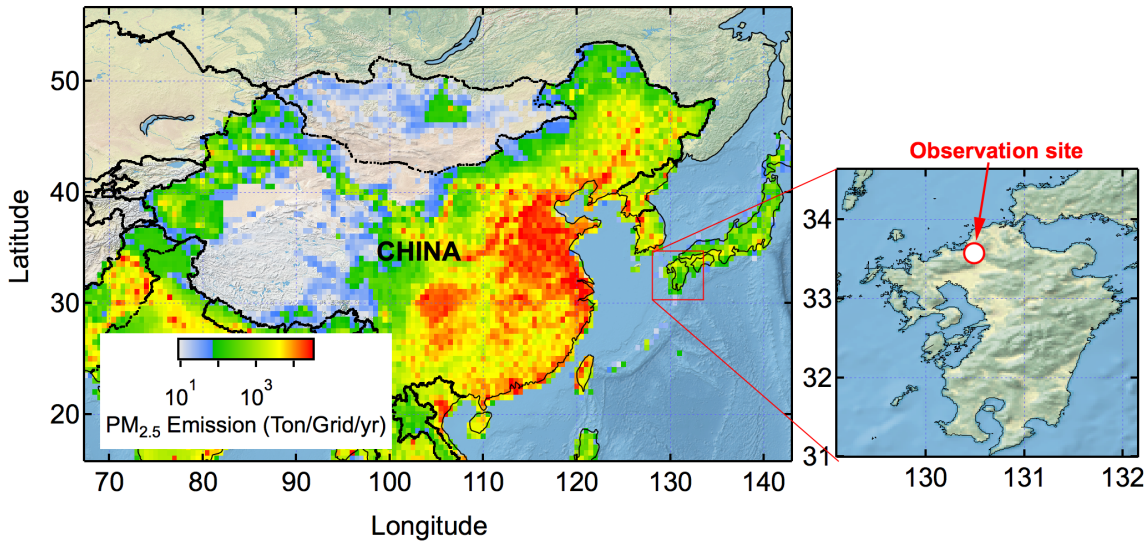

455

456 Figure 1. Geographic location of the observation site and annual anthropogenic emissions of
457 primary $PM_{2.5}$ in East Asia according to REAS2.0 emission inventory (Ohara *et al.,* 2007).

458

459

460

461

462

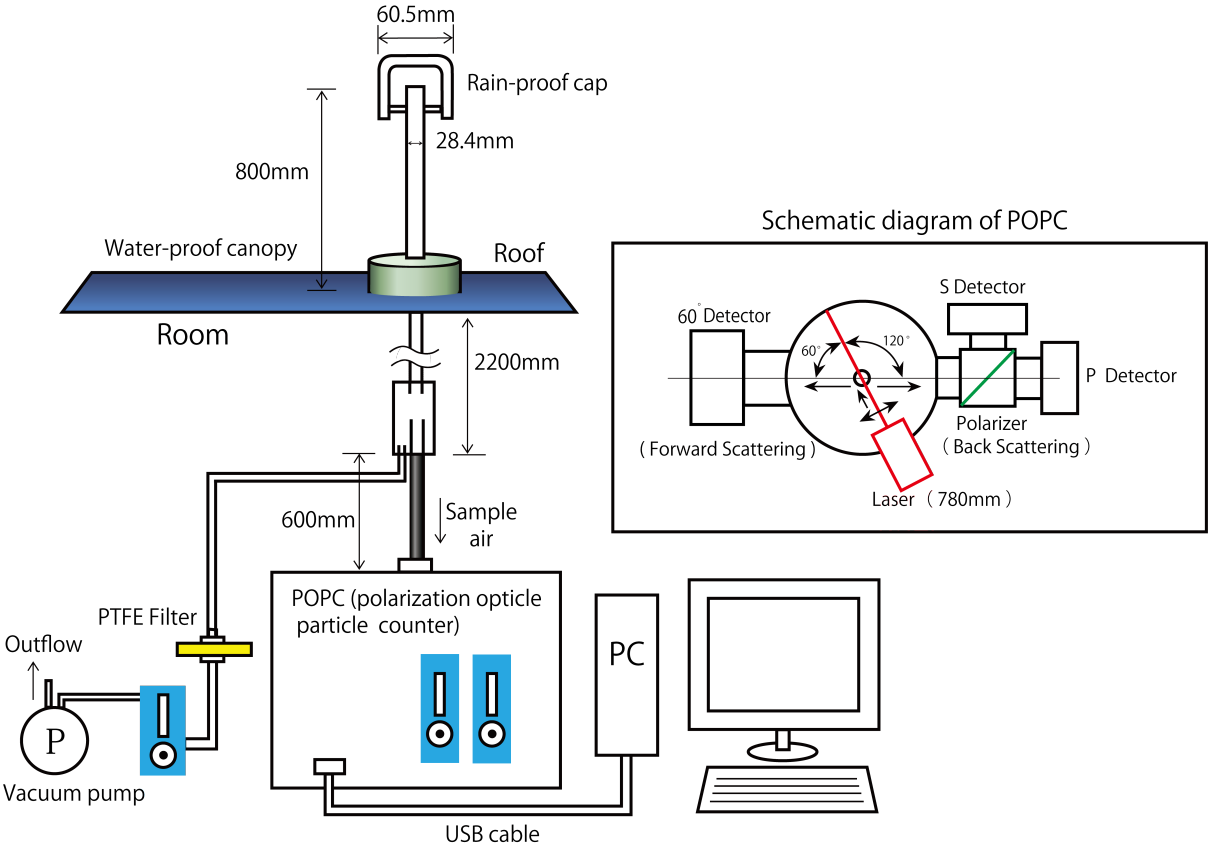

Figure 2. The layout of the instrument and schematic diagram of the polarization optical particle counter (POPC).

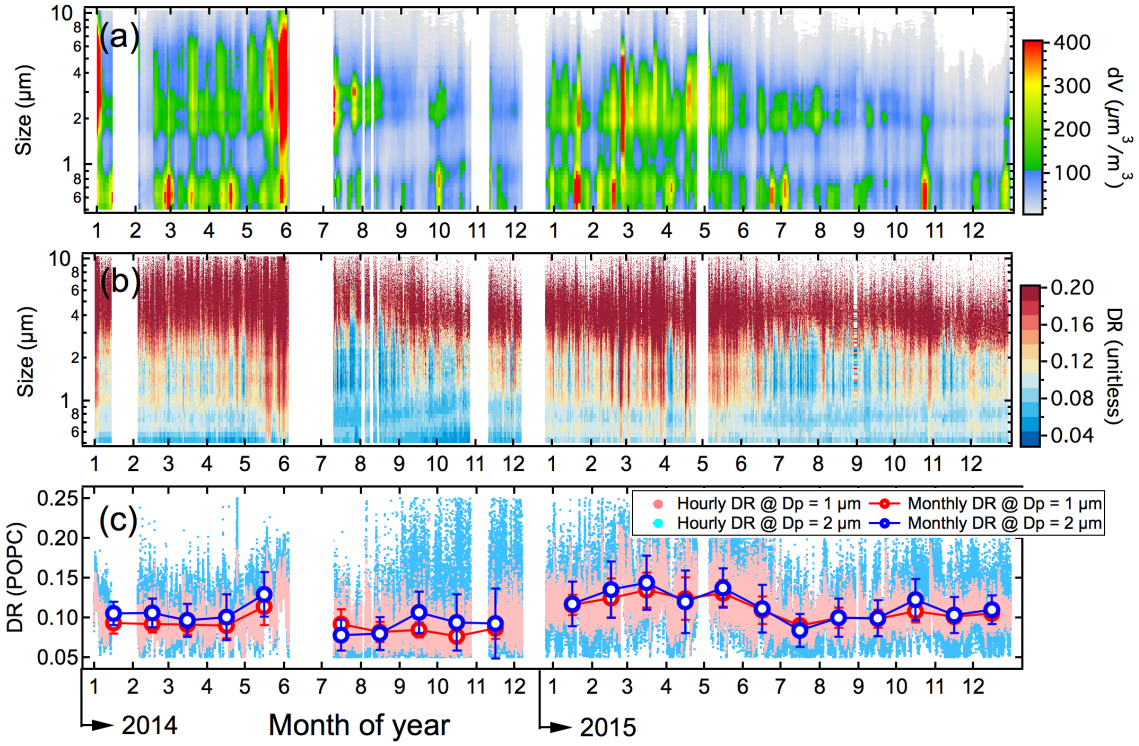

Figure 3. Time series of (a) volume size distributions, (b) depolarization ratio, and (c) monthly averaged depolarization ratio for the particles at D_p = 1 μm and D_p =2 μm in 2014 and 2015.

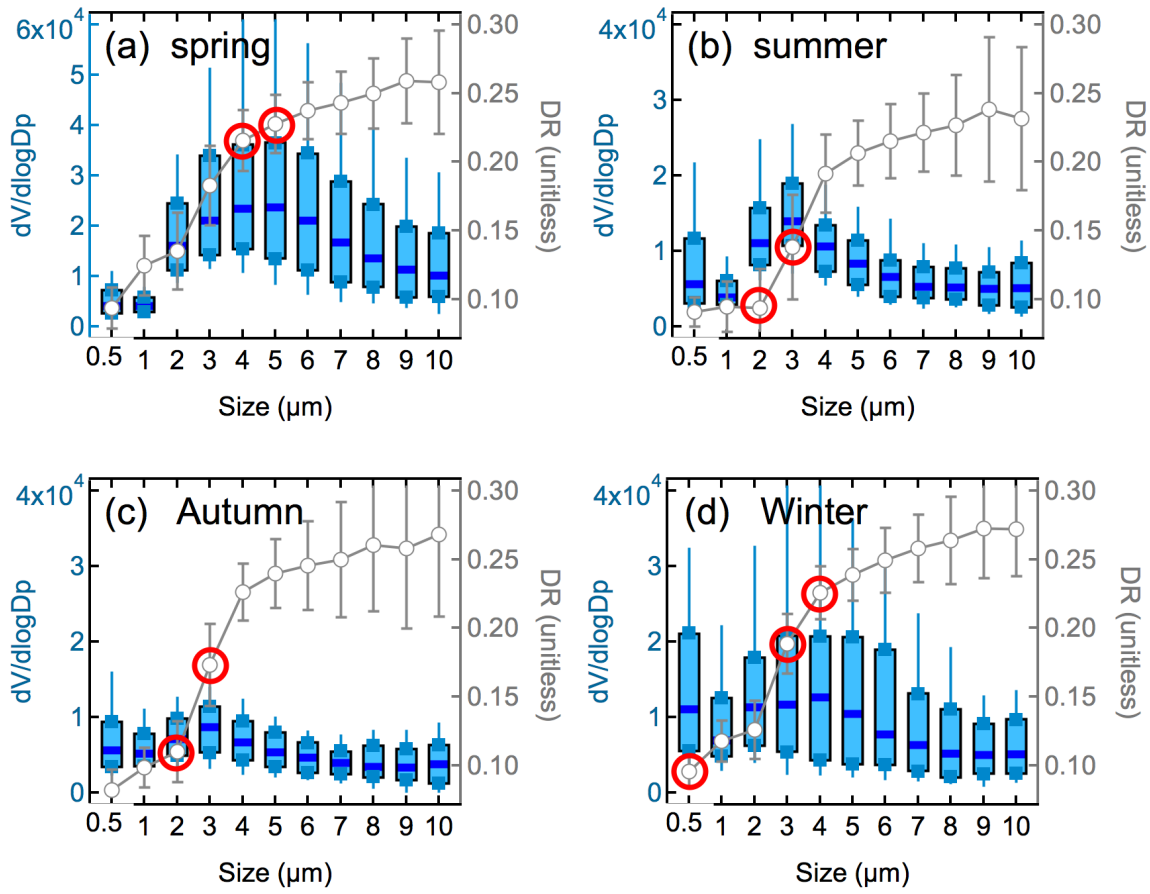

475

476 Figure 4. Volume size distribution (left axis) and size-dependent depolarization ratio (right
477 axis) of aerosols in (a) spring (March, April, May: MAM), (b) summer (June, July, August:
478 JJA), (c) autumn (September, October, November: SON), and (d) winter (December, January,
479 February: DJF). The box and whiskers in the plot represent the 10th, 25th, 75th, 90th percentiles
480 and median values, and the red circles represent the corresponding DR values for the peak
481 size range in the volume size distribution.

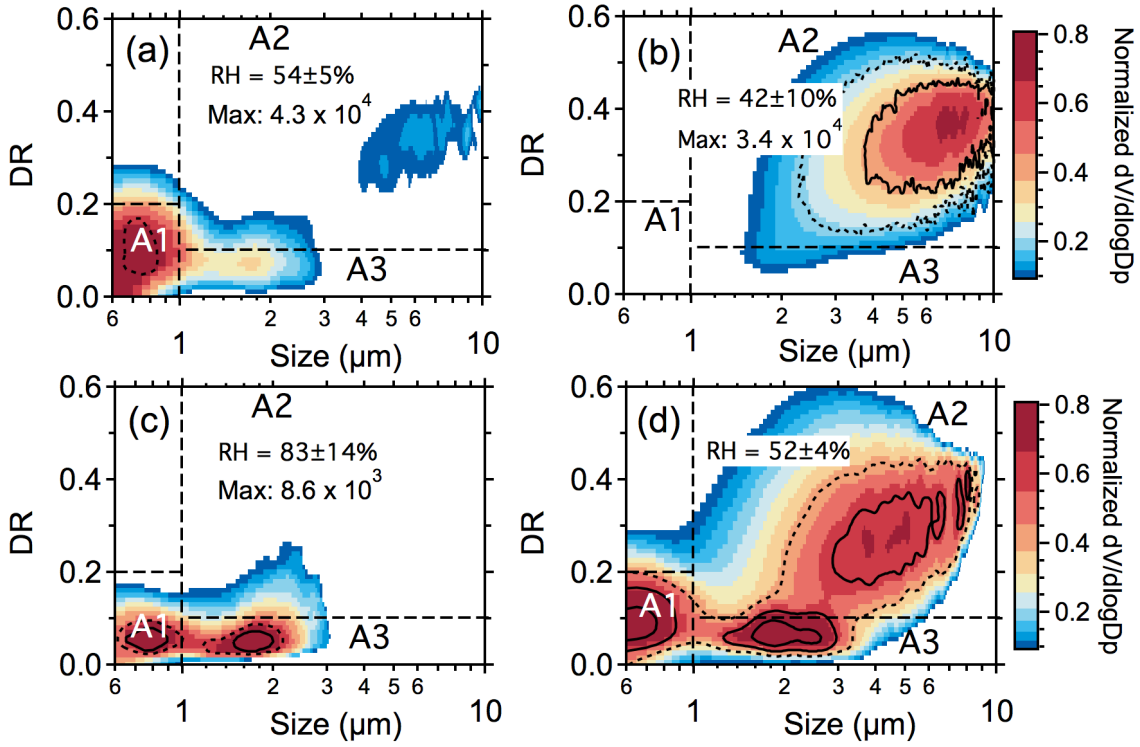

482

483 Figure 5. Variation in the depolarization ratio as a function of particle size for (a)
484 anthropogenic-pollution-dominant, (b) mineral-dust-dominant, (c) typhoon influenced, and
485 (d) mixed aerosol types. Colors represent normalized volume concentrations (maximum
486 value = 1). The relative humidity (RH, from the Japan Meteorological Agency,
487 http://www.jma.go.jp/jma/index.html) values in the plot are the means for each period.

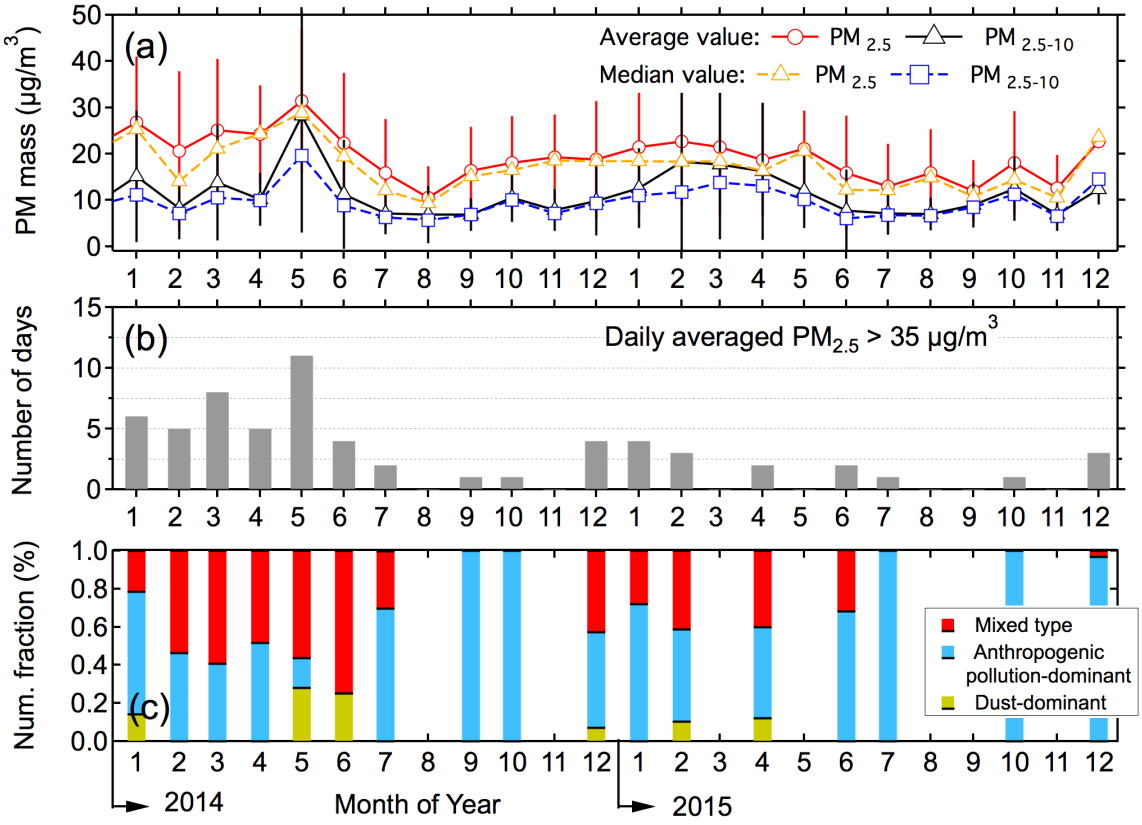

Figure 6. (a) The monthly mean and median values of mass concentrations of $PM_{2.5}$ and $PM_{2.5\text{-}10}$, (b) number of days, with daily averaged mass concentrations of $PM_{2.5}$ exceeding 35 $\mu g/m^3$ (the National Ambient Air Quality Standard (NAAQS) of $PM_{2.5}$ in Japan), and (c) contributions of different aerosol types to substandard air quality days at the site during the observation period.

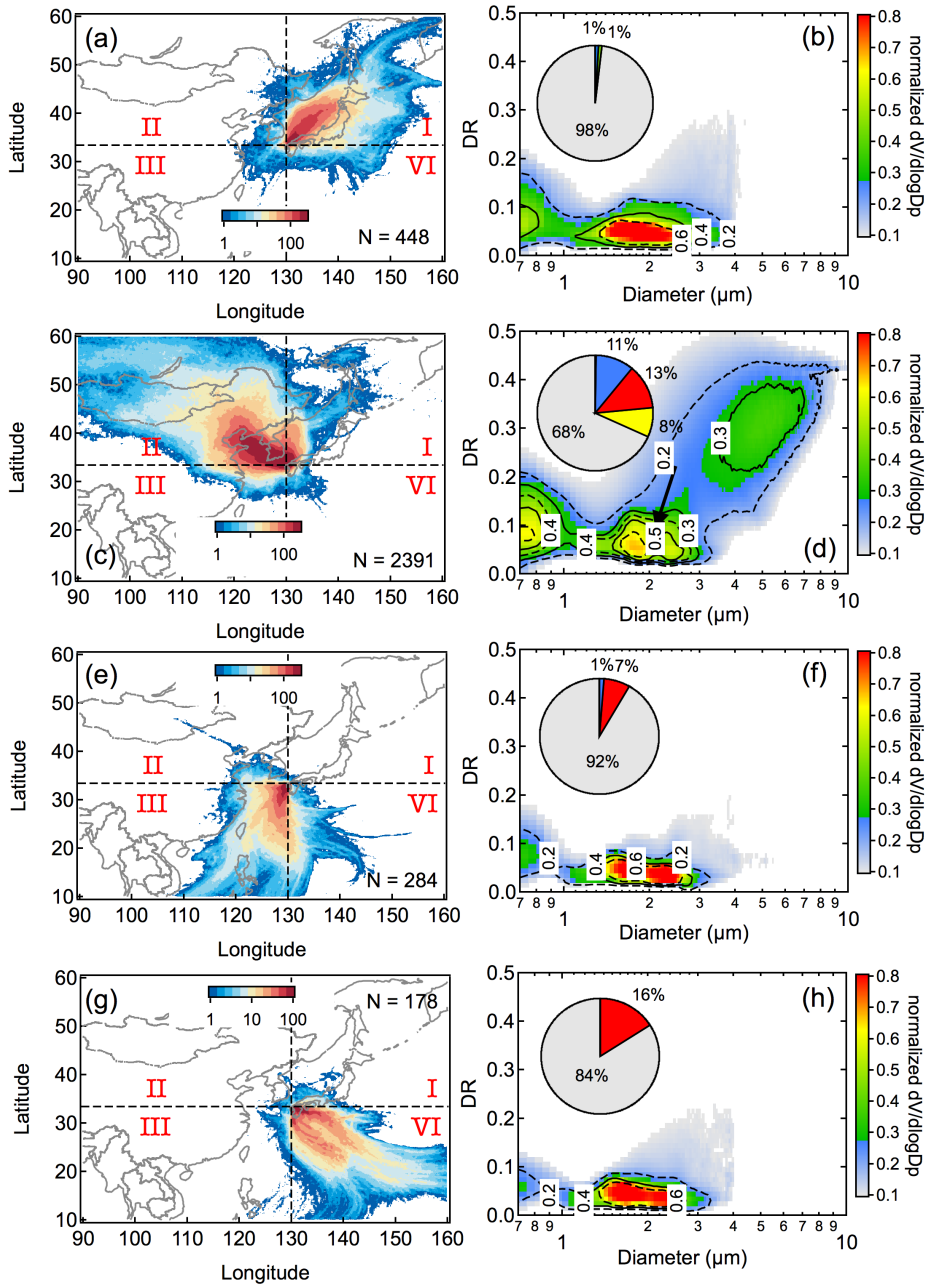

494

495 Figure 7. Air masses arriving at the observation site, originating from (a) Region I, (c)
496 Region II, (e) Region III and (g) Region IV. The color scale represents the total number
497 (logarithmic scale) of trajectories that passed through the mixed layer of the target grid. The
498 N value indicates the total hours in each scenario, and the total number of trajectories actually
499 is N value multiplied by 27 because of ensemble simulations for each run. The corresponding
500 size-resolved depolarization characteristics of transported particles are shown in (b), (d), (f),
501 and (h). Gray in the pie chart indicates the number fraction of days that meet the air quality
502 standard. Red, yellow, and blue indicate the number fractions of substandard air quality days
503 caused by anthropogenic-pollution-dominant, mineral-dust-dominant, and mixed-type-
504 dominant scenarios, respectively.

505

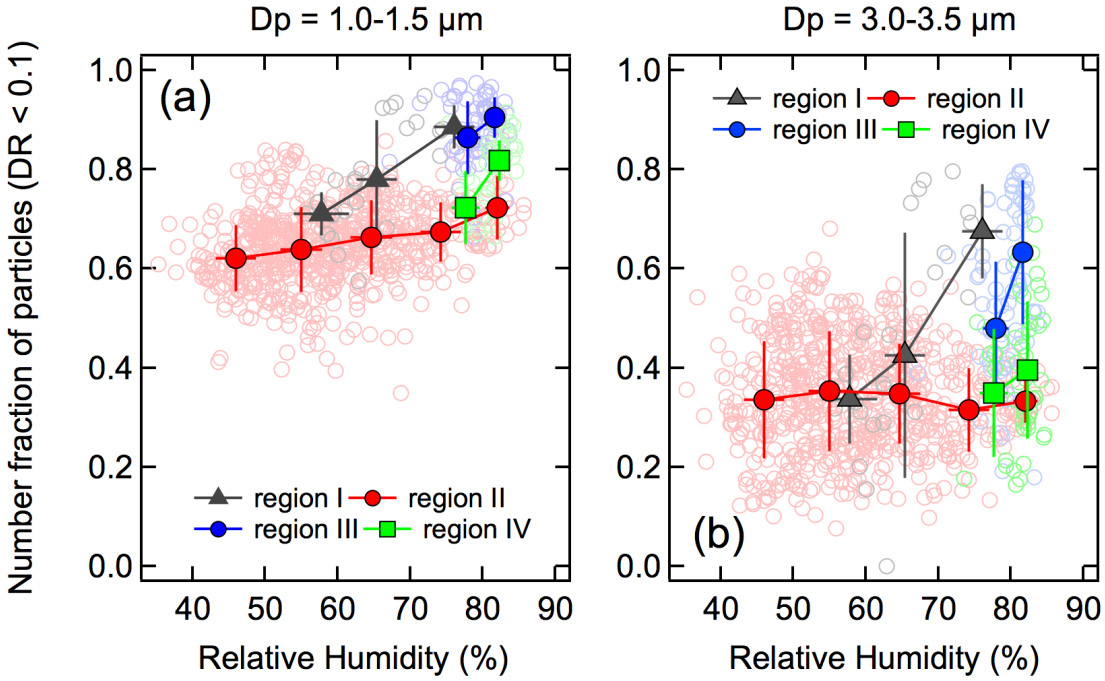

506

507 Figure 8. Scatter plots of the dependence of the number fraction of particles (DR <0.1) as a
508 function of relative humidity for different size ranges (a) 1.0-1.5 μm and (b) 3.0-3.5 μm. The
509 light-colored circles in the background of the plot are the original data used for performing
510 the statistical analyses.